ACTA PHYSICA POLONICA A No. 6 Vol. **145** (2024)

Role of Mn Doping in Improving the Hydrophobic Property of ZnO Coating on Aluminum Substrate

Z. Belamri[a,*], N. Mermoul[a] and D. Hamana[a,b]

[a] *Phase Transformation Laboratory, Frères Mentouri Constantine 1 University, RN 79, Constantine 25000, Algeria*

[b] *Laboratory of Advanced Materials Technology, Ecole Nationale Polytechnique de Constantine, BP 79A Ali Mendjeli, Constantine 25000, Algeria*

Received: 07.07.2023 & Accepted: 08.03.2024

Doi: 10.12693/APhysPolA.145.301

*e-mail: belamri.zehira@umc.edu.dz

Due to their interesting physical and structural characteristics, zinc oxide nanostructures are one of the most commonly used materials to elaborate hydrophobic or superhydrophobic surfaces. In this work, undoped and Mn-doped ZnO thin films are prepared by the thermal oxidation of electrodeposited zinc thin layers on aluminum substrates. Structural analysis by X-ray powder diffraction and Raman spectroscopy shows the formation of ZnO mico-nanostructures, and no secondary phase linked to Mn is detected. Energy dispersive X-ray spectroscopy analysis confirms the presence of zinc and oxygen, with no Mn element detected in the doped samples. However, at high Mn concentrations, Raman spectroscopy shows the main ZnO modes with a decrease in their intensities and the appearance of new modes with increasing Mn concentration, indicating that the structural quality is slightly degraded. The formation of the deformed flower-shaped structures covered with spherical ZnO nanostructures leads to the hydrophobicity of the ZnO coating, and doping with a small Mn concentration improves this last property.

topics: hydrophobic property, electrodeposition, thermal oxidation, Mn-doped ZnO

1. Introduction

Zinc oxide (ZnO) is commonly used in the form of powder, bulk, and thin films for technological and commercial applications [1–3]. Due to its hydrophobic affinity, nanostructured ZnO is also considered as a good self-cleaning coating because of the low surface free energy of the (002) planes in the wurtzite structure [4]. Surface hydrophobicity is determined by a combination of its chemical, topographic, and microstructural properties. A flat surface with low surface energy is known to have a high contact angle (CA) with water, i.e., between 100 and 120°. However, this is insufficient to produce a superhydrophobic surface, which requires a water contact angle greater than 150°. If a surface is rough or micro-textured with low interfacial free energy, the contact angle with water can reach almost 180° and the surface will remain dry [5]. These surfaces are better suited for coatings on substrates made of glass for electro–optical applications like solar cells [6]. However, there are some other applications of this coating on metallic materials; it can be used for satellite antennas, billboards, and high-voltage lines because it has good self-cleaning properties [7], anti-adherence to snow or ice, etc. [8–10].

Aluminum is one of these metallic materials, which has been a crucial material for study in recent times due to its abundance in nature, ease of handling, and numerous industrial applications, particularly in the aerospace and local industries [11, 12], packaging, building construction (windows, doors, etc.), household items (cooking utensils), electronics (transmission lines, substrate materials, light-emitting diode (LED) support, etc.), chemistry, optical coating, and mirrors [13]. A significant disadvantage for these applications is that aluminum corrodes easily, especially in aqueous conditions with Cl^- ions, even in trace concentrations of Cl^- [14]. Therefore, creating a hydrophobic or superhydrophobic coating for this material is essential. Previous research has demonstrated that the application of superhydrophobic coating is an efficient corrosion prevention strategy [15]. Among these materials used as coating thin films is zinc oxide (ZnO).

ZnO coatings can be synthesized in a variety of ways. The particular needs of the application, the intended thickness, the homogeneity of the film, the surface states, and the equipment and resources available all play a role in the selection of the synthesis process. Electrodeposition is one of the simple and easy techniques for producing ZnO thin layers; this is a process where charged colloidal particles suspended in a liquid medium are deposited under the influence of an electric field and accumulate on the surface of the electrode. This method offers appropriate and controllable ways to elaborate composite films on a variety of substrates, such as altering the applied voltage and the electrolyte composition [16]. Furthermore, it is the most widely used and inexpensive method of producing surface roughness on metal.

The majority of scientific publications describe the process of modifying ZnO films for coatings. Examples of such modifications include adjusting the Zn:O ratio and changing the electrolyte solution composition, temperature, and electric potential [17–19]. Yin et al. [20] successfully produced a superhydrophobic coating on aluminum alloy by anodization process and chemical modification, utilizing zinc oxide (ZnO) nanoparticles suspended in alcohols at different bath temperatures and functionalized with stearic acid. In another study, the authors used electrodeposition of copper on aluminum surfaces and electrochemical modification with organic molecules containing stearic acid to generate superhydrophobic aluminum surfaces [21]. Hassan et al. [22] worked on the development of superhydrophobic surfaces using magnesium nanoparticles for catalytic applications and achieved excellent properties on the aluminum substrate along with a high-water contact angle of 160° and a low sliding angle of 2° via etching, immersion, and annealing method. By changing a coating formulation based on hydrophilic silica nanoparticles and poly(acrylic acid) (PAA), it is possible to observe how particle loading affected the wetting qualities of coatings and how an increase in particle loading increased wettability [23]. Da Silva et al. [24] fabricated a low-cost superhydrophobic coating on 5052 aluminum alloy using a combination of methods. By the applied methodology, they are able to achieve superhydrophobic coatings with a contact angle of 164° and sliding angles of 1°. Corrosion inhibitors and surface modification can be dangerous and have an adverse effect on the environment. They are also expensive and time-consuming. To prevent metal corrosion, it is therefore essential to develop easy, inexpensive, non-toxic, and environmentally friendly surface treatment methods. In this context, recently, we fabricated a hydrophobic ZnO coating on aluminum substrates easily by thermal oxidation using the electrodeposition method. We show the impact of oxidation time or temperature on the morphological and structural characteristics and hydrophobic property of the obtained ZnO thin films [25, 26].

In this paper, we aim to improve the hydrophobic property of ZnO coating on an aluminum substrate by the addition of the Mn element, using a low-cost and simple electroplating technique. ZnO is chosen for deposition as a thin film due to its excellent physical and non-toxic properties. Also, it is found that ZnO thin films can be superhydrophobic without any low surface energy passivation layers [27–29]. The effect of doping concentration on the structural and physical properties of ZnO thin films elaborated by the thermal oxidation technique on aluminum substrates has been studied.

TABLE I

Used precursors and optimum conditions for the deposition of pure and MZnO thin films.

Parameters	Optimized values
Zn acetate solution concentration	0.2 mol/l
Mn concentration	0. 01, 0.5, 2, 4, and 6%
bath temperature	25°C
solution quantity	40 ml
distance between two electrodes	1.5 cm
DC voltage	−10 V
deposition time	15 min
annealing temperature	500°C

2. Experiment

2.1. Substrate preparation

In this present work, aluminum is chosen as a substrate due to its many good properties that give it a great advantage in many industrial applications. Before deposition, the substrates undergo mechanical polishing until the desired surface shape and thickness of 2 mm are obtained. After that, the substrates are cleaned ultrasonically for 15 min in a methanol and distilled water bath, respectively.

2.2. Experimental conditions

Zinc acetate dihydrate powder ($Zn(CH_3COO)_2$–$2H_2O$) precursor is first dissolved in distilled water to prepare the starting solution with a molarity of 0.2 mol/l for the deposition of undoped Zn thin films. For Mn-doped ZnO layers, manganese acetate ($Mn(CH_3COO)_2$) is added to the base solution with different concentrations (Table I). The deposition of the studied thin films is carried out at a low temperature with agitation in order to speed up the reaction on the substrate and make it possible to increase the deposition rate and improve the quality of the resulting films. This is performed at −10 V for 15 min, with respect to the distance between the aluminum substrate (cathode) and the platinum electrode (anode) of 1.5 cm. Undoped and Mn-doped ZnO thin films are obtained by thermal oxidation at 500°C for 2 h of electroplated Zn layers in a tubular furnace. Table I summarizes the various parameters optimized in this work.

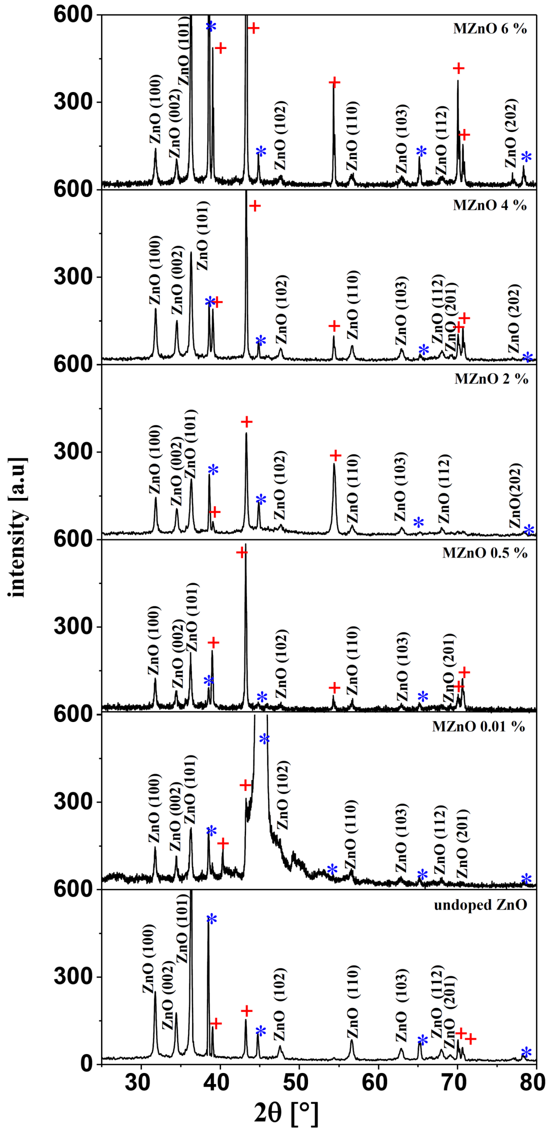

Fig. 1. XRD spectra of pure and MZnO thin films with different Mn concentrations (* — Al and + — Zn).

The present phases and their orientations are examined using a Panalytical Empyrean diffractometer (X-ray powder diffractometer (XRD), Cu K_α radiation, $\lambda = 1.540$ Å, in the range from 10° to 80°). Raman spectra are recorded using a HORIBA LabRAM HR Evolution spectrometer at room temperature with a monochromatic radiation source of 473 nm. The morphological and elemental analyses are performed using a field emission gun scanning electron microscope (FEG-SEM)(Jeol JSM-7100F) equipped with energy dispersive X-ray spectrometer (EDX). The contact angle measurements are carried out 5 s after the deposition of a water drop with a volume of 5 μL on the elaborated thin films using a LEYBOLD light source (6 V, 30 W) and a projection lens, which allows the static image of the drop displayed on a 30×30 cm^2 screen to be enlarged.

3. Structural characterizations

3.1. X-ray diffraction study of undoped and Mn-doped ZnO thin films

The X-ray diffraction is performed on undoped and Mn-doped ZnO thin films (MZnO). The dopant concentrations vary in the range of 0.01–6%, by keeping all other deposition parameters constant during the deposition. The obtained spectra (Fig. 1) of pure and MZnO thin films reveal that all elaborated thin films are polycrystalline. They show multiple peaks corresponding to (100), (002), (101), (102), (110), (103), (112), (201), and (202) planes related to the hexagonal wurtzite crystal structure (according to ICDD card No. 01-070-2551). All diffraction spectra show a major peak (101) located around 36.298°, highlighting the preferential direction of elaborated ZnO thin films. Regardless of the doping concentration, all the spectra of elaborated films show peaks similar to pure ZnO, and no new peaks associated with Mn oxides appear. This confirms the successful substitutional replacement of Mn ions in Zn sites of the ZnO lattice. It is also observed from the XRD patterns that there is a decrease in some peak intensities (especially the intensity of (101) peak) at lower doping concentrations ($\leq 4\%$ Mn) and an increase in (101) peak intensity for 6% Mn compared with that of undoped ZnO. This can be explained by the variation of crystallite size which is calculated using the Scherrer formula [30]

$$D = \frac{K\lambda}{\beta \cos(\theta_B)}, \tag{1}$$

where K is a constant known as a shape factor ($K = 0.94$), λ is the X-ray wavelength of 1.5406 Å, θ_B is the Bragg diffraction angle, and β is the FWHM (full width at half maximum) of θ_B.

At lower Mn concentrations, the decrease in the crystallite size (see Table II) is due to strain caused by the incorporation of manganese ions into zinc ion sites, accompanied by a decrease in diffraction peak intensity; this effect is also observed in other previous studies [31].

However, it can be seen that at the Mn concentration of 6%, the opposite effect occurs. This variation in peak intensity shows the doping concentration effect on the surface texture of the studied thin films. Additionally, coexisting transition metal ions in the ZnO matrix can promote grain coalescence by raising the electrostatic energy and decreasing the energy barrier needed for grain boundary motion [32].

Usually, the number of dislocations per unit area determines the dislocation density in the thin film. These values show the quality of the films and defect states in a given material. By knowing the crystallite size, the dislocation density (δ) can be

TABLE II

Structural parameters of pure and MZnO thin films treated for 2 h at 500°C.

Samples	$2\theta_{101}$ [°]	FWHM [°]	Crystallite size D [nm]	Dislocation density δ ($\times10^{15}$) [ligne/m^2]	Lattice deformation ε ($\times10^{-3}$)
pure ZnO	36.299	0.225	39	0.664	0.9329
0.01% Mn	36.263	0.315	28	1.302	1.3062
0.5% Mn	36.240	0.257	34	0.866	1.0658
2% Mn	36.319	0.324	27	1.377	1.3433
4% Mn	36.278	0.297	29	1.157	1.,2315
6% Mn	36.280	0.184	47	0.444	0.7629

determined using Williamson and Smallman's formula for the (101) plane [31]

$$\delta = \frac{1}{D^2}, \tag{2}$$

where D is the average crystallite size.

Microstrain (ε) of the prepared ZnO films is calculated using the following equation [31]

$$\varepsilon = \frac{\beta\cos(\theta)}{4}, \tag{3}$$

where β is the FWHM.

The dislocation density and the microstrain values are found to increase for low Mn concentration compared with a pure sample (Table II). However, for high doping concentrations (6% and 4% Mn), these parameters decrease due to the increase in crystallite size. This is mainly linked, firstly, to the increase in grain boundaries for low doping concentration (D is minimal), and secondly, to the distortion of the ZnO host lattice due to external factors. Mn^{+2} impurities reduce the nucleation and subsequent growth rate of the ZnO nanostructure [31]. In order to stabilize the crystal structure, the crystallite size decreases to release the internal strain [33].

The stress state of the prepared thin films can be determined using XRD spectra. The biaxial stress e_{zz} along the c axis perpendicular to the substrate plane is calculated from the lattice parameter c [34], i.e.,

$$e_{zz} = \frac{C - C_0}{C_0}\,100\%, \tag{4}$$

where c is the lattice parameter of the elaborated ZnO films and C_0 (0.5207 nm) is the unstrained ZnO lattice parameter.

The residual stress σ parallel to the thin film surface is expressed as [34]

$$\sigma = \frac{2C_{13}^2 - C_{33}(C_{11}+C_{12})}{2C_{13}}\,\frac{C - C_0}{C_0}. \tag{5}$$

Here, C_{ij} are the elastic stiffness constants for single crystal ZnO ($C_{11} = 208.8$ GPa, $C_{33} = 213.8$ GPa, $C_{12} = 119.7$ GPa, $C_{13} = 114.2$ GPa). According to the previous relations, we find a link between the biaxial stress e_{zz} and the residual stress σ

$$\sigma = -233\,e_{zz}. \tag{6}$$

TABLE III

Values of c, e_{zz}, and σ for pure and MZnO thin films treated for 2 h at 500°C.

Samples	e_{zz} [%]	σ [GPa]	c [Å]
pure ZnO	−0.0400	0.0932	5.2062
0.01%	−0.0759	0.1769	5.2055
0.5%	−0.0055	0.0129	5.2069
2%	−0.5522	1.2868	5.1955
4%	−0.4865	1.1336	5.1973
6%	−0.4134	0.9633	5.1987

Note that they have the opposite direction in the interface plane of the layer and the substrate [35]. This shows the advantage of measuring the c parameter since it allows us to know the state of the stress in different directions in elaborated thin films. The strain can be positive (tensile) or negative (compressive).

Table III shows the stress values for elaborated thin films. The negative sign of e_{zz} indicates that the films are under compressive stress along the c axis, accompanying the positive values of residual stress; the latter confirms that the films undergo an attractive force parallel to the substrate surface caused by impurities (doping elements), defects (decrease in vacancies), and lattice distortions (growth of grain) in the crystal.

3.2. Raman spectroscopy study of undoped and Mn-doped ZnO thin films

Raman spectra are more sensitive to crystallinity, structural disorder, and defects of nanostructures. The vibration properties of ZnO thin films doped with manganese are investigated by the Raman scattering technique in this work.

The Raman spectra of pure and Mn-doped ZnO thin films treated for 2 h at 500°C are presented in Fig. 2. For low Mn concentrations (0.01% and 0.5%), one can observe five peaks: E_2^{low}, $E_2^{(\text{high})}-E_2^{(\text{low})}$, A_1(TO), E_2^{high}, and A_1(LO)/E$_1$(LO). These peaks correspond to the

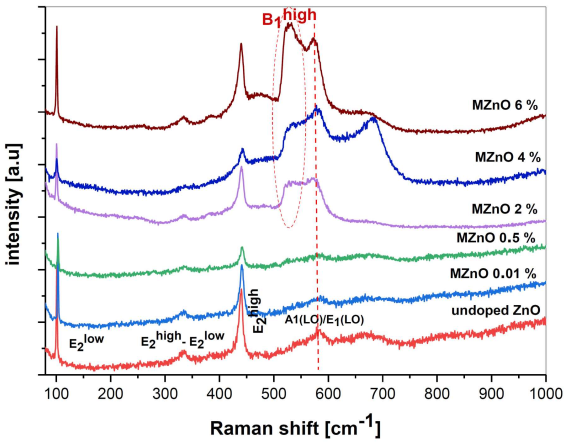

Fig. 2. Raman spectra of undoped ZnO and MZnO thin films treated for 2 h at 500°C; the doping percentage is indicated inside the curves.

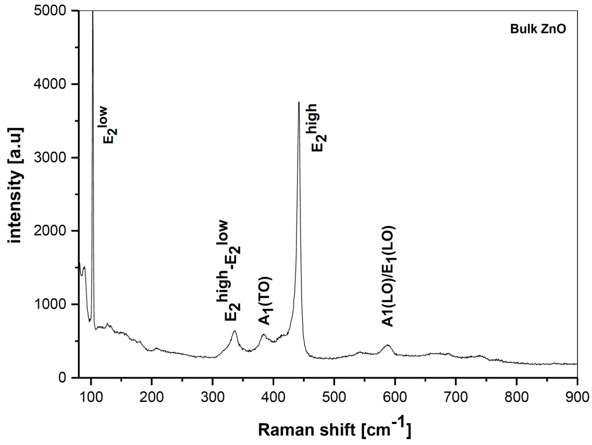

Fig. 3. Raman spectra of bulk ZnO as a reference.

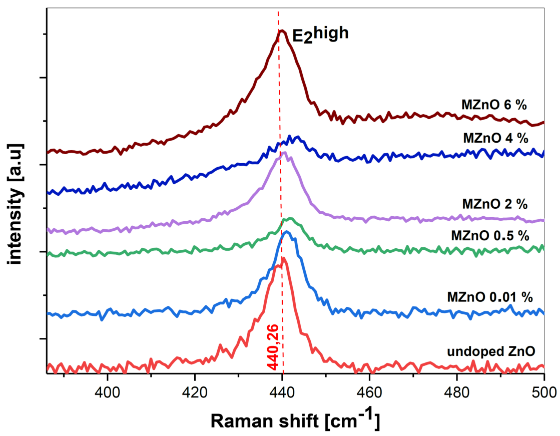

Fig. 4. Superposition of the E_2^{high} Raman peak of MZnO thin layers treated for 2 h at 500°C; the doping percentage is indicated inside the curves.

hexagonal ZnO phonon modes, as compared with bulk ZnO (Fig. 3). The high intensity of the E_2^{high} peak for the studied samples is related to the vibration of the oxygen atom sublattice in the ZnO crystal [36, 37], which reflects the crystallization quality of the ZnO thin films of the hexagonal wurtzite structure [38]. This confirms the obtained results of the DRX analysis. The shift of this peak toward a lower or higher wavenumber is due to the chemical bonds and symmetry of the atoms [39]. Hence, changes in chemical bond length cause a wave number shift due to Mn doping into the ZnO lattice. It was found that the E_2^{high} peak position is very sensitive to the intrinsic residual stress of the material [40, 41]; moreover, the previously calculated values of the residual stress show that as the MZnO thin films are under attractive force ($\sigma > 0$) parallel to the substrate surface, the E_2^{high} peak shifts to higher wavenumbers with an increase in the Mn concentration (Fig. 4). For high Mn concentrations (2%, 4%, and 6% Mn), the main peaks of the undoped ZnO lattice are still visible, although the shape of the Raman spectrum changes, indicating that the structural quality is slightly degraded. We note the appearance of a new vibration near the A_1(LO)/E$_1$(LO) modes of the hexagonal ZnO between 500 cm^{-1} and 740 cm^{-1} called B_1^{high} silent mode [42, 43].

4. Morphological characterization of the studied ZnO thin films

Different atomic rearrangement processes involved during the thermal oxidation of undoped and Mn-doped ZnO thin films on the aluminum substrates are responsible for the different surface topographies of these studied layers. Figure 5a–c shows the micrographs obtained by the field emission gun scanning electron microscope (FEG-SEM) and the corresponding EDX pattern (Fig. 6a–c) of the studied samples. Figure 5a confirms that the undoped ZnO thin film exhibits a compact morphology with needle-shaped nanostructures attached to each other, whose thickness is reduced with height. However, the surface morphology changed with manganese doping. FEG-SEM images show slightly deformed flower-shaped structures (conical or spherical shape) formed on the surface of MZnO thin film with 0.01% Mn. These deformed flowers are covered with a large number of nanostructured spherical ZnO (inset image with a large magnification in Fig. 5b shows nanostructured spherical ZnO), which roughens the surface of elaborate thin layers. When the Mn concentration increases to 6%, the density of the spherical and conical particles increases (Fig. 5c). Elemental analysis by EDS shows the presence of zinc and oxygen in ZnO thin film, and no Mn element was detected in doped samples, which can be due to the low among of the Mn doping element (Fig. 6b–c).

5. Wettability study of elaborated ZnO thin films: Measurements of hydrophobicity

The wetting properties of elaborated ZnO thin films are analyzed by measuring the contact angle (CA) with water of these studied layers, as shown in Fig. 7a–f. Measurements show that the obtained contact angle is 120.9° for undoped ZnO (Fig. 7a). The shape of the droplets is more spherical (Fig. 7a), which indicates that the undoped ZnO film structure is inherently hydrophobic. Therefore, the water contact angle value is related to the surface morphology and Mn-doped ZnO coating. The larger contact angle in the MZnO thin films (0.01% and 0.5% Mn), which enhanced from 120.91° in pure ZnO to 135° in the MZnO thin films (Fig. 7a–c), has been linked to the higher roughness of these films due to the presence of microstructural conical flowers (≈ 1 μm) that are organized in specific configurations and form rough surfaces, making it possible to trap air in the holes between the hierarchical structures and prevent water from spreading on the surface. According to the Cassie–Baxter model [44], in this case, the liquid droplet sits

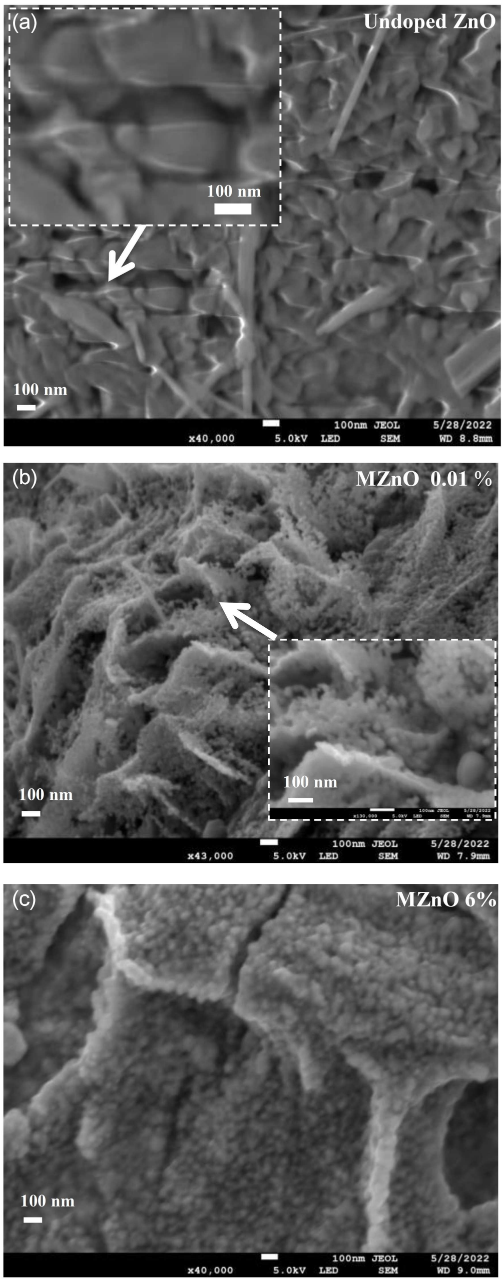

Fig. 5. FEG-SEM images of ZnO thin films: (a) undoped ZnO (inset image zoom shows spherical or conical shape), (b) 0.01% Mn, (c) 6% Mn (inset image with a high-magnification).

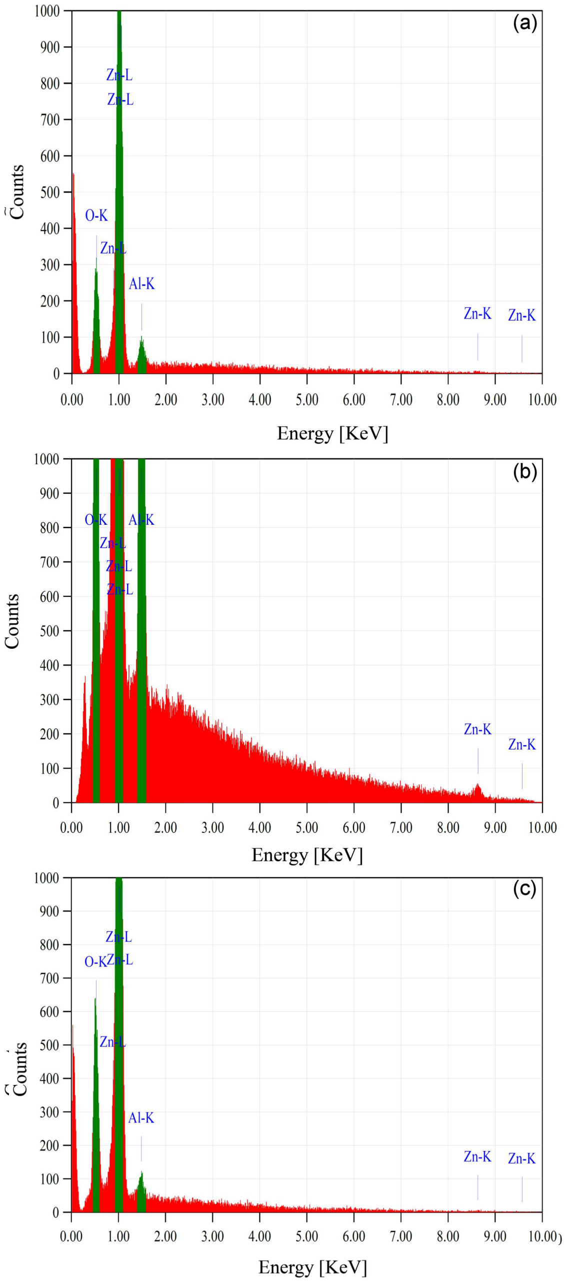

Fig. 6. EDX analysis of ZnO thin films: (a) undoped ZnO, (b) 0.01% Mn, (c) 6% Mn with suitable indexing.

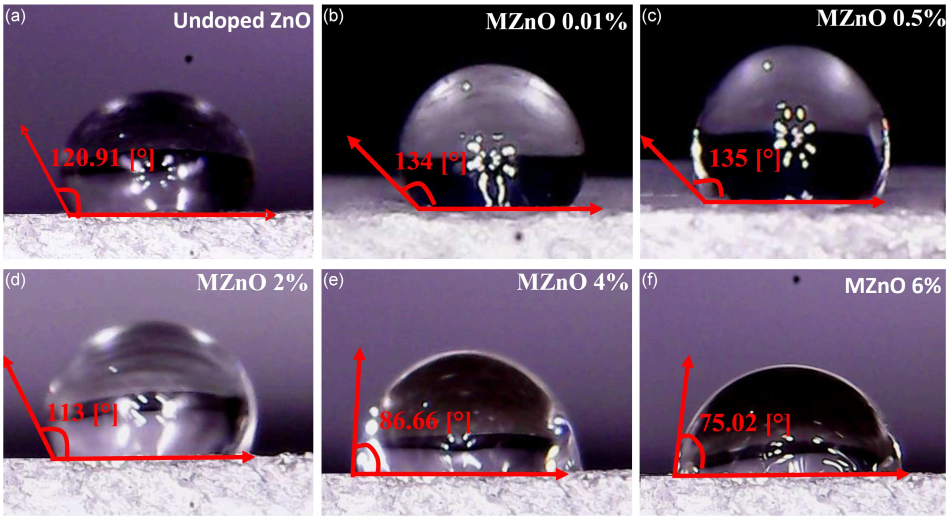

Fig. 7. Contact angle with water of the studied samples: pure ZnO (a) and MZnO thin films, (b) 0.01% Mn, (c) 0.5% Mn, (d) 2% Mn, (e) 4% Mn, and (f) 6% Mn.

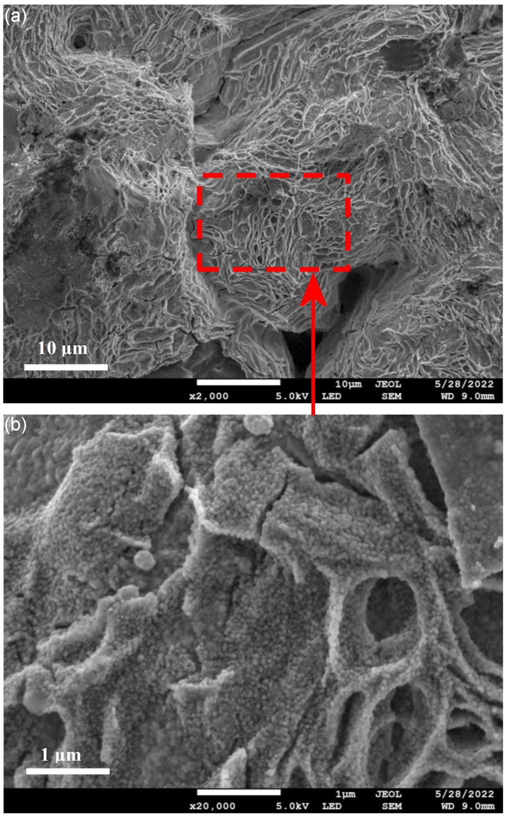

Fig. 8. FEG-SEM images of Mn-doped ZnO thin film (6% Mn): (a) low-magnification FEG-SEM image, (b) high-magnification FEG-SEM image.

on the maximum of the crest, so the hydrophobicity increases. The presence of transition metals such as Mn in the ZnO structure can reduce the surface energy of the gains, which is made possible by additional transition metal dopant porters [32]. So, doping ZnO thin films on aluminum with low Mn concentrations leads to an increase in the hydrophobic property.

Otherwise, highly Mn-doped ZnO (4% and 6% Mn) leads to a decrease in the contact angle, and the surface becomes hydrophilic (Fig. 7e and f). This may be linked to the reduced surface roughness of the ZnO film due to the existence of micropores (Fig. 8). The high-magnification FEG-SEM image of the 6% MZnO sample (Fig. 8b) clearly shows the self-aggregation of several nanocrystals, which leads to the formation of mesovoids, and to the generation of micropores. This indicates that the doped ZnO thin films with high Mn concentrations conduct a high affinity for crystalline grains to coalesce, which helps the increase in grain boundaries and pores. Self-aggregation phenomena were observed in a previous study. The authors focused on the elaboration of pure and doped ZnO nanoclusters and the determination of their internal porosity [45]. In this work, the surface of the studied MZnO sample (6%) is porous, exhibiting mesovoids (Fig. 8). The pores are irregular in shape and randomly distributed everywhere in the spherical structure. The presence of porosity permits the dispersion of the water molecules in the pores of the films.

6. Conclusions

The objective of this work is to elaborate pure and Mn-doped ZnO thin films with different Mn concentrations obtained by thermal oxidation of electrodeposited Zn on aluminum substrate. The study is devoted to the effect of doping on the morphology of the thin film and the crystallite size, which in turn affects the hydrophobicity of the ZnO coating.

Structural characterization by XRD shows that the synthesized ZnO thin films crystallize into hexagonal wurtzite structure with a preferential orientation along (101) whether ZnO is pure or Mn-doped. The comparison of the obtained results shows that the thermally oxidized MZnO thin films present a preferential growth direction along the (101) axis, low dislocation density, and low deformation. However, for higher Mn concentrations, a few degradations of the host lattice appear by distorting the local atomic order around the impurities.

The Mn-doped ZnO thin films with low Mn concentration exhibit a deformed flower-like structure (spherical or conical shape). These deformed flowers are covered with a large number of ZnO nanoparticles, which roughens the surface of elaborate thin films and leads to the best hydrophobicity among the studied films. Doping ZnO thin films with high Mn concentrations leads to grain coalescence and the generation of pores, which contribute to surface hydrophilicity.

In summary, the simple and low-cost technique of thermal oxidation at 500°C in air of electroplated Zn layers has been demonstrated as a very economical and effective technique for the synthesis of ZnO nanostructures on metallic aluminum substrate. ZnO surfaces are hydrophobic in their pure state, and when they are doped with low Mn concentrations, this property is improved.

References

[1] E. Asikuzun, O. Ozturk, L. Arda, C. Terzioglu, *J. Mol. Struct.* **1165**, 1 (2018).

[2] J. Marquina, E. Quintero, F. Ruette, Y. Bentarcurt, *Chin. J. Phys* **63**, 63 (2020).

[3] B. Rahal, B. Boudine, Y. Larbah, L. Guerbous, M. Sebais, O. Halimi, M. Siad, *Optik* **169**, 303 (2018).

[4] P.W. Chi, C.W. Su, D.H. Wei, *Appl. Surf. Sci.* **404**, 380 (2017).

[5] Y. Huang, D.K. Sarkar, X.-G. Chen, *Appl Surf Sci.* **356**, 1024 (2015).

[6] F. Ghahramanifard, A. Rouhollahi, O. Fazlolahzadeh, *Superlattices Microstruct.* **114**, 1 (2018).

[7] B. Yin, L. Fang, A. Tang, Q. Huang, J. Hu, J. Mao, G. Bai, H. Bai, *Appl. Surf. Sci.* **258**, 580 (2011).

[8] D. K Sarkar, M. Farzaneh, *J. Adhes. Sci. Technol.* **23**, 1215 (2009).

[9] D. Quéré, *Rep. Prog. Phys.* **68**, 2495 (2005).

[10] T. Kako, A. Nakajima, H. Irie, Z. Kato, K. Uematsu, T. Watanabe, K. Hashimoto, *J. Mater. Sci.* **39**, 547 (2004).

[11] P.C.R. Varma, P. Periyat, M. Oubaha, C. Mcdonagh, B. Duffy, *Surf. Coat. Technol.* **205**, 3992 (2011).

[12] A.M. Abdel-Gaber, B.A. Abd-El-Nabey, I.M. Sidahmed, A.M. El-Zayady, M. Saadawy, *Mater. Chem. Phys.* **98**, 291 (2006).

[13] L. Torrisi, C. Scolaro, *Acta. Phys. Pol. A* **128**, 48 (2015).

[14] W.A. Badawy, F.M. Al-Kharafi, A.S. El-Azab, *Corros. Sci.* **41**, 709 (1999).

[15] B. Yin, L. Fang, J. Hu, A.Q. Tang, W.H. Wei, J. He, *Appl. Surf. Sci.* **257**, 1666 (2010).

[16] M. Moradi, R. Saidi, B. Hoomehr, K. Raeissi, *Ceram. Int.* **49**, 9239 (2023).

[17] G. Acikbas, H. Hindi, *J. Inorg. Organomet. Polym.* **34**, 419 (2024).

[18] O.A.A. El-Shamy, M.A. Deyab, *Mater. Lett.* **331**, 133402 (2023).

[19] S. Özcan, G. Açıkbaş, N.Ç. Açıkbaş, *Appl. Surf. Sci.* **438**, 136 (2023).

[20] B. Yin, L. Fang, A. Tang, Q. Huang, J. Hu, J. Mao, G. Bai, H. Bai, *Appl. Surf. Sci.* **258**, 580 (2011).

[21] Y. Huang, D.K. Sarkar, X.-G. Chen, *Nano-Micro Lett.* **3**, 160 (2011).

[22] N. Hassan, M.M. Fadhali, S. Al-Sulaimi et al., *J. Mol. Liq.* **383**, 122085 (2023).

[23] S. Turkoglu, J. Zhang, H. Dodiuk, S. Kenig, J.A. Ratto, J. Mead. *Polymers* **14**, 4553 (2022).

[24] R.G.C. da Silva, M.I.C. Malta, L.A.P. de Carvalho, J.J. da Silva, W.L.C. da Silva Filho, S.H. Oliveira, E.G. de Araújo, S.L. Urtiga Filho, M.R.S. Vieira, *Surf. Coat. Technol.* **457**, 129293 (2023).

[25] Z. Belamri, L. Boumaza, S. Boudjadar, *Phys. Scr.* **98**, 125949 (2023).

[26] Z. Belamri, W. Darenfad, N. Guermat, *J. Nano-Electron. Phys.* **15**, 02026 (2023).

[27] M. Laurenti, V. Cauda, R. Gazia, M. Fontana, V.F. Rivera, S. Bianco, G. Canavese, *Eur. J. Inorg. Chem.* **14**, 2520 (2013).

[28] N.L. Tarwal, P.S. Patil, *Appl. Surf. Sci.* **256**, 7451 (2010).

[29] N.L. Tarwal, A.V. Rajgure, A.I. Inamdar, R.S. Devan, I.Y. Kim, S.S. Suryavanshi, Y.R. Ma, J.H. Kim, P.S. Patil, *Sens. Actuators A Phys.* **199**, 67 (2013).

[30] A. Mahroug, S. Boudjadar, S. Hamrit, L. Guerbous, *J. Mater. Sci. Mater. Electron.* **25**, 4967 (2014).

[31] S. Balamurali, S. Saravanakumar, R. Chandramohan, P.N. Magudeswaran, *Braz. J. Phys* **51**, 1502 (2021).

[32] A. Derri, M. Guezzoul, A. Mokadem, A. Ouerdane, K.B. Bensassi, M. Bouslama, B. Kharoubi, E. Hameurlaine, *Opt. Mater.* **145**, 114467 (2023).

[33] B. Singh, S. B. Shrivastava, V. Ganesan, *Int. J. Nanosci.* **15**, 1650024 (2016).

[34] T.P. Rao, M.S. Kumar, S.A. Angayarkanni, M. Ashok, *J. Alloys Compd.* **485**, 413 (2009).

[35] Z. Sofiani, B. Derkowska, P. Dalasinski et al., *Opt. Commun.* **267**, 439 (2006).

[36] S. Prasad, S. Bansal, S.P. Pandey, *Mater. Today Proc.* **49**, 3022 (2022).

[37] B. Hadžić, N. Romčević, M. Romčević, I. Kuryliszyn-Kudelska, W. Dobrowolski, U. Narkiewicz, D. Sibera, *Opt. Mater.* **58**, 317 (2016).

[38] M. Silambarasan, S. Saravanan, T. Soga, *e-J. Surf. Sci. Nanotechnol.* **12**, 286 (2014).

[39] N.D. Raskar, D.V. Dake, V.A. Mane, E. Stathatos, U. Deshpande, B. Dole, *J. Mater. Sci. Mater. Electron.* **30**, 895 (2019).

[40] C.B. Ong, L.Y. Ng, A.W. Mohammad, *Renew. Sustain. Energy Rev.* **81**, 551 (2018).

[41] M.M. Obeid, H. R. Jappor, K. Al-Marzoki, I.A. Al-Hydary, S.J. Edrees, M.M. Shukur, *RSC Adv.* **9**, 332 (2019).

[42] F.J. Manjón, B. Marí, J. Serrano, A.H. Romero, *J. Appl. Phys.* **97**, 53516 (2005).

[43] W.E. Fenwick, M.H. Kane, R. Varatharajan et al., *Proc. SPIE* **6474**, 64741Q (2007).

[44] S. Hosseini, H. Savaloni, M. Gholipour-Shahraki, *J. Theor. Appl. Phys.* **11**, 1 (2017).

[45] K.C. Barick, S. Singh, M. Aslam, D. Bahadur, *Microporous and Mesoporous Mater.* **134**, 195 (2010).